Modes of action of the archaeal Mre11/Rad50 DNA-repair complex revealed by fast-scan atomic force microscopy

Ekaterina Zabolotnaya[a] [ID], Ioanna Mela[a] [ID], Mark J. Williamson[b] [ID], Sian M. Bray[c], Siu Kei Yau[d], Dimitra Papatziamou[d], J. Michael Edwardson[a], Nicholas P. Robinson[d,1] [ID], and Robert M. Henderson[a,1]

[a]Department of Pharmacology, University of Cambridge, CB2 1PD Cambridge, United Kingdom; [b]Department of Chemistry, University of Cambridge, CB2 1EW Cambridge, United Kingdom; [c]Department of Biochemistry, University of Cambridge, CB2 1QW Cambridge, United Kingdom; and [d]Department of Biomedical and Life Sciences, Faculty of Health and Medicine, Lancaster University, LA1 4YG Lancaster, United Kingdom

Mre11 and Rad50 (M/R) proteins are part of an evolutionarily conserved macromolecular apparatus that maintains genomic integrity through repair pathways. Prior structural studies have revealed that this apparatus is extremely dynamic, displaying flexibility in the long coiled-coil regions of Rad50, a member of the structural maintenance of chromosome (SMC) superfamily of ATPases. However, many details of the mechanics of M/R chromosomal manipulation during DNA-repair events remain unclear. Here, we investigate the properties of the thermostable M/R complex from the archaeon *Sulfolobus acidocaldarius* using atomic force microscopy (AFM) to understand how this macromolecular machinery orchestrates DNA repair. While previous studies have observed canonical interactions between the globular domains of M/R and DNA, we observe transient interactions between DNA substrates and the Rad50 coiled coils. Fast-scan AFM videos (at 1–2 frames per second) of M/R complexes reveal that these interactions result in manipulation and translocation of the DNA substrates. Our study also shows dramatic and unprecedented ATP-dependent DNA unwinding events by the M/R complex, which extend hundreds of base pairs in length. Supported by molecular dynamic simulations, we propose a model for M/R recognition at DNA breaks in which the Rad50 coiled coils aid movement along DNA substrates until a DNA end is encountered, after which the DNA unwinding activity potentiates the downstream homologous recombination (HR)-mediated DNA repair.

homologous recombination | atomic force microscopy | DNA repair | protein–nucleic acid interaction

The Mre11/Rad50 (M/R) DNA-repair complex is an essential molecular machine critical for cellular viability and chromosomal maintenance and is conserved in all divisions of life; the bacteria, archaea and eukaryotes (1–5). The robust and stoichiometric association of the Mre11 nuclease and the Rad50 ATPase ensures that they function together to coordinate the recognition and subsequent processing of DNA damage during the initial stages of DNA repair (4, 6, 7). This chromosomal surveillance apparatus is one of the first complexes to be recruited to cytotoxic DNA double-strand breaks (DSBs) (8, 9) and acts both as a DNA-damage sensor and also as a key driver of the DNA-damage response (8–10).

Insight into how the M/R machinery senses and processes broken chromosomes has been provided by structural studies in which thermophilic archaeal homologs of M/R are used (2, 4, 6, 11–14). These investigations have shown that the M/R assembly is dynamic, alternating between dramatically contrasting "open" and "closed" structural conformations, mediated by movements within the globular tetrameric core of the complex. This globular core, which consists of a dimer of Mre11 and Rad50 dimers, has well-established roles in the interaction with the DNA substrates (15, 16). The binding, hydrolysis, and release of ATP at the Rad50 catalytic sites drive the transition between these two opposing states, thereby influencing the accessibility of DNA substrates to the catalytic regions of Mre11 and Rad50 (15–17).

In addition to catalytic roles, the M/R complex also performs essential architectural functions to mediate chromosomal bridging and tethering during the repair events. Rad50 proteins belong to the structural maintenance of chromosome (SMC) superfamily of ATPases (18, 19), which includes the condensins and cohesins in eukaryotes (20, 21), and MukB and RecN in prokaryotes (22). SMC proteins are characterized by two globular ATPase domains, located at the N- and C-termini, which are separated by long antiparallel coiled-coil regions. These regions bend around a central feature of SMC proteins known as the "hinge" region (23), or the analogous but structurally distinct "zinc-hook" region located in Rad50 proteins (24), bringing the two globular domains together. Unique to the Rad50 family, this zinc-hook region harbors cysteine residues in a "CXXC" motif that is capable of coordinating zinc ions (24). The two Rad50 zinc hooks within one tetrameric complex can interact intramolecularly via coordination of a central zinc ion to form a closed ring structure reminiscent of cognate SMC closed-ring arrangements (24–27). Alternatively, the Rad50 zinc-hook interactions can occur intermolecularly to tether the two ends of the DNA break or to facilitate the pairing of the two homologous chromosomes during the homologous repair

Significance

The Mre11/Rad50 (M/R) complex forms the core of an essential DNA-repair complex, conserved in all divisions of life. Here we investigate this complex from the thermophilic archaeon *Sulfolobus acidocaldarius* using real-time atomic force microscopy. We demonstrate that the coiled-coil regions of Rad50 facilitate M/R interaction with DNA and permit substrate translocation until a free end is encountered. We also observe that the M/R complex drives unprecedented unwinding of the DNA duplexes. Taking these findings together, we provide a model for how the M/R complex can identify DNA double-strand breaks and orchestrate repair events.

(HR)-mediated repair event (4). Atomic force microscopy (AFM) and electron microscopy studies of M/R complexes have revealed that the Rad50 coiled coils undergo dramatic and long-range rearrangements upon either DNA binding or ATP hydrolysis and promote intermolecular connections to establish chromosomal tethering (24, 28–30). Furthermore, long-range allosteric communication between the ATPase domains and the hook/hinge regions via the coiled-coil regions (11) seems to play important roles in the biological functions of both the complexes and the cognate SMC proteins (23, 31).

In this study, we use fast-scan AFM (FS-AFM; 1–2 frames per second) in fluid to examine the M/R complex from the thermophilic crenarchaeote *Sulfolobus acidocaldarius* to gain insights into the dynamic molecular interactions of the complex with DNA. Our data reveal that archaeal complexes use the Rad50 coiled-coil regions adjacent to the zinc-hook apex to bind to, manipulate, and traverse linear double-strand DNA (dsDNA) molecules until the substrate termini (equivalent to DSBs) are identified. We investigate these binding events further by molecular dynamics (MD) simulations, which confirm that the wild-type (WT) M/R is capable of tracking along dsDNA using its Rad50 zinc-hook apex. Our study provides insights into a newly established DNA-tracking activity of the complex (32) which helps explain how the complex locates to DNA ends and DSBs. Our analyses also reveal that this archaeal DNA-repair complex can drive an unprecedented degree of unwinding of DNA duplex templates in an ATP-dependent manner. On the basis of our observations, we propose a model of M/R action during DSB break repair. We suggest that M/R complexes can act together during DNA repair to coordinate identification of the DSB by traversing to the DNA end while concomitantly unwinding the homologous chromosome to facilitate the strand-invasion steps of HR.

Results

Structural Analyses of the Archaeal Mre11/Rad50 Complex from *S. acidocaldarius* Using AFM Imaging in Fluid.
We report four different classes of architectural arrangements for the *S. acidocaldarius* Mre11/Rad50 (M/R) complex (Fig. 1 *A, i–iv*). In the first class, the two Rad50 coiled coils protruded from the globular tetrameric core of the complex but these did not join

intramolecularly via the zinc hooks, adopting a "winged" conformation (Fig. 1 *A, i*). In the second arrangement, the Rad50 coiled coils again protruded from the globular domains of the tetramer, but the coiled-coil apices associated intramolecularly at the zinc hooks to form a closed "ring" shape (Fig. 1 *A, ii*). The third "dumbbell" conformation was a distinct architectural arrangement in which two distal M/R heterodimeric globular domains were observed, connected by the long coiled-coil regions via the zinc hooks; the two globular M/R domains remained separated in this conformation (Fig. 1 *A, iii*). Without the dimerization at the zinc hooks, the dumbbell form is reduced to the fourth conformation, a "half-dumbbell" arrangement (representative of single heterodimers) (Fig. 1 *A, iv*). Furthermore, M/R oligomers consisting of multiple heterotetramers in the ring or winged conformations were observed in our study of the *S. acidocaldarius* complex (e.g., an oligomer of five heterotetramers in the ring arrangement is displayed in Fig. 1 *A, v*). A gel filtration profile and analysis of the oligomeric state of M/R complexes using SEC-MALS (size exclusion chromatography–multiangle light scattering) and volume analysis from AFM data are incorporated in *SI Appendix*, Fig. S1, Table S1, and Note S1. *SI Appendix*, Table S2 quantifies the number of particles in different arrangements. A comparison of the oligomerization among different species appears in *SI Appendix*, Table S3.

Measurement of the individual and connected Rad50 coiled coils (Fig. 1*B*) showed the length of an individual Rad50 coiled coil and two connected coiled coils to match their predicted lengths (full details in legend to Fig. 1).

Archaeal M/R Localization at DNA Ends and DNA Tethering Is Facilitated by the Rad50 Coiled Coils.
The interaction of the wild-type M/R complexes with a linear dsDNA substrate was visualized by AFM imaging in dry conditions after incubation in the presence or absence of 3 mM adenosine triphosphate (ATP) or nonhydrolyzable ATP analog adenosine 5′-(β, γ-imido) triphosphate (AMP-PNP) (Fig. 2). The wild-type complex showed similar binding events onto the DNA substrate under three different experimental regimes (buffer only, 3 mM ATP, 3 mM AMP-PNP) (Fig. 2 *A–C*). DNA binding occurred via the globular catalytic head of the protein complex, with the coiled coils of Rad50 commonly extending from the DNA substrates (Fig. 2 *A–C*).
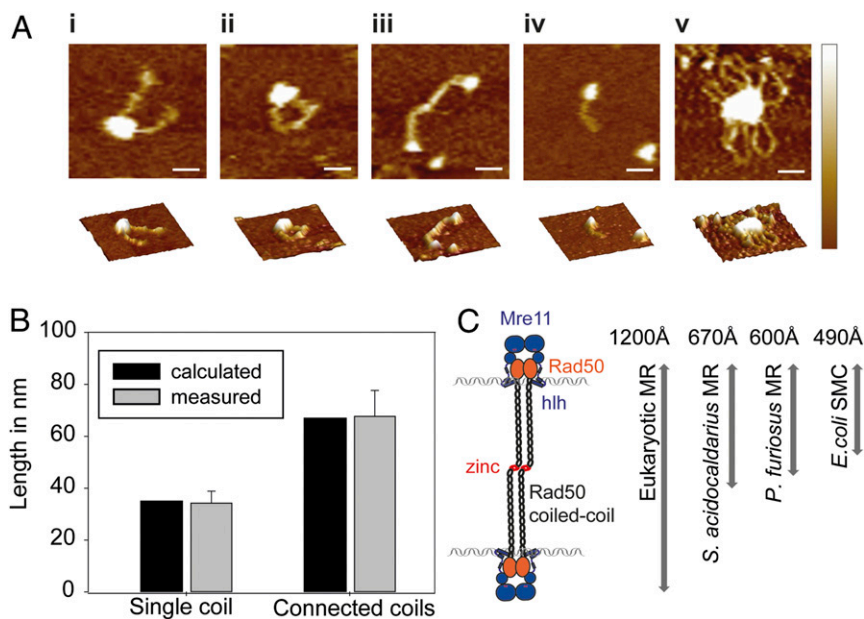
Fig. 1. Structural analyses of the *S. acidocaldarius* Mre11/Rad50 complex using AFM imaging in fluid. (*A, i–v*) *S. acidocaldarius* Mre11/Rad50 (M/R) heterotetramer molecules display four different architectural arrangements and also higher-order oligomers. Two-dimensional (*Top*) and three-dimensional (*Bottom*) AFM images of each individual structure: (*i*) winged, (*ii*) ring, (*iii*) dumbbell, (*iv*) half-dumbbell arrangements, and (*v*) oligomeric form. (Scale bar: 20 nm.) (Height scale bar: 2 nm [dark to light].) (*B*) Comparison of the calculated (black) and measured (gray) length of the Rad50 coiled coils. Measured length of an individual Rad50 coiled coil (n = 100) is 34.18 ± 4.64 nm; length of two connected coiled coils (n = 106) is 67.67 ± 10 nm, each result resembles the calculated lengths of 35.1 and 67 nm, respectively. (*C*) Distances (measured by EM or AFM) between two DNA strands, if bridged by connected Rad50 coiled coils from different species: (*Left* to *Right*) Eukaryotic Rad50 ~1,200 Å; *P. furiosus* Rad50 ~600 Å; *S. acidocaldarius* Rad50 ~670 Å; and bacterial SMC protein MukB from *E. coli* ~490 Å.
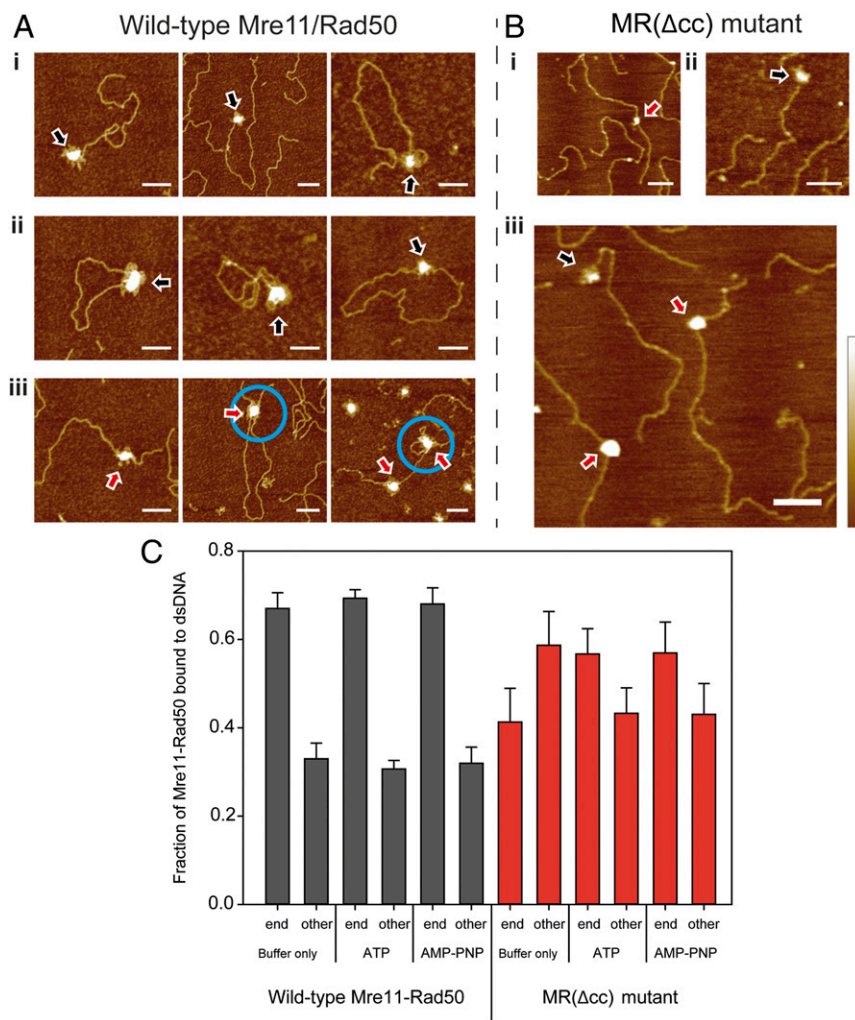
Fig. 2. Wild-type Mre11/Rad50 binds primarily to DNA ends via the globular domains. (*A*, *i–iii*) *S. acidocaldarius* wild-type Mre11/Rad50 (M/R) hetero-tetramer molecules binding to linear dsDNA. Three types of binding event are observed (*A–C*), in either the presence or absence of ATP or AMP-PNP: (*i*) M/R (black arrow) located at an open DNA end; (*ii*) M/R (black arrow) binding joins the two ends of a DNA molecule forming a closed circle; (*iii*) M/R (red arrow) bound at an internal location on the DNA template. *Middle* example shows an M/R complex creating an extended dsDNA loop by contacting two internal sites on the same DNA molecule (blue circle). *Right*, shows a similar but smaller dsDNA loop (blue circle) formed when the complex binds to sites located closer together than in the first example. (*B*, *i–iii*) The Rad50 coiled-coil truncated mutant MR(Δcc) binds to linear dsDNA (3 kb) at both free DNA ends and internal locations along the duplex. Images depict DNA-binding reactions in the presence of 3 mM AMP-PNP. Black arrows (*ii* and *iii*) indicate MR(Δcc) situated at free dsDNA ends. Red arrows (*i* and *iii*) point to mutant complexes associating with other internal locations. (Scale bar in *A* and *B*: 100 nm.) (Height scale bar, 2 nm [dark to light].) (*C*) Bar chart showing the binding location (DNA end or other location along the linear dsDNA) of the wild-type *S. acidocaldarius* Mre11/Rad50 heterotetramer (gray) and the MR(Δcc) mutant (red), in reaction buffer, or in the presence of 3 mM ATP or AMP-PNP. Error bars represent SEM.

A volume analysis to quantify the number of wild-type complexes in different events shown in Fig. 2*A* appears in *SI Appendix*, Fig. S2*A* and Note S2.

These DNA-binding events were classified into three distinct groups (Fig. 2 *A*, *i–iii*). In the first group, the M/R complex bound at the ends of the linear DNA substrate (Fig. 2 *A*, *i*). In the second group, the wild-type complexes bound to the two opposing ends of the linear DNA duplex and associated to form a closed DNA circle (Fig. 2 *A*, *ii*). Interestingly, we only observed

bridging between the two DNA ends when assemblies of several complexes were present (33). In the last group, the M/R complex bound to the linear DNA template at internal regions other than the free DNA ends (Fig. 2 *A*, *iii*). Within this group, $35 \pm 5\%$ of the wild-type complexes ($n = 746$) interacted with the same DNA substrate at more than one position (blue circles in Fig. 2*A*, *iii*) and these associations resulted in the formation of dsDNA loops of various sizes. Crucially, in addition to the DNA binding of M/R complexes via intermolecular zinc-hook associations that
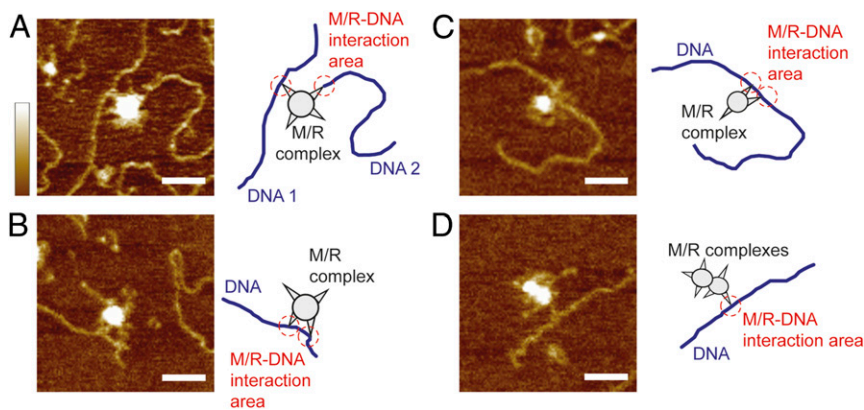
Fig. 3. (*A–D*) Associations of the M/R complex with DNA substrates via the Rad50 coiled-coil apices. Wild-type Mre11/Rad50 (M/R) complexes tethering DNA through Rad50 coiled-coil apices. The Rad50 coiled coils protrude from the globular part of the M/R complex and extend toward the DNA template. Red circles in the cartoon models highlight the location of the M/R–DNA interaction through coiled coils. (Scale bar: 50 nm.) (Height scale bar: 2 nm [dark to light].)

have been described previously, we also observed direct DNA-binding events between the coiled-coil regions of Rad50 and the DNA substrate (described below).

For each of the three experiments, the binding location of the M/R molecules along the DNA substrates was determined by measuring the distance from the DNA end to the location of the bound protein complex (Fig. 2C). In each of the conditions, the proportion of M/R molecules that bound at the free DNA ends was significantly higher than the number that bound to "internal" nonend regions of the DNA duplex (numeric details in *SI Appendix*, Note S3).

These DNA-binding investigations were next repeated using a mutant M/R complex MR(Δcc) (with truncated coiled coils where the native zinc-hook region is still present) (Fig. 2 B, i–iii and Fig. 2C). This complex was capable of associating with the free DNA ends and could also bind at internal locations along the substrate (Fig. 2 B, i–iii). In contrast to results for the wild-type complex, no statistically significant preference for binding to free dsDNA ends was observed for the MR(Δcc) mutant, regardless of the buffer conditions used (Fig. 2C; numeric details in *SI Appendix*, Note S3). Interestingly, the increased propensity for the WT complex to locate to DNA ends when compared with the MR(Δcc) complex suggests that the full-length coiled-coil domains are important for the observed distribution at the DNA ends. Furthermore, the MR(Δcc) complexes failed to form the DNA loops or bridges between two or more DNA ends, that we observed with the full-length WT complex analyses (Fig. 2 A, ii and iii). This confirms that full-length Rad50 coiled coils are required to tether two DNA ends together (17, 24, 34).

Real-Time FS-AFM Imaging of DNA Binding of the Archaeal Mre11/Rad50 Complex via the Coiled-Coil Apices.

In addition to the canonical DNA binding via the catalytic globular M/R domain, we also observed unexpected interactions of M/R complexes with DNA via their coiled-coil apices (Fig. 3 A–D). In these instances, the Rad50 coiled coils extended from the globular part of the complex and their apices interacted with the DNA, in some instances tethering two DNA molecules when M/R oligomers assembled (Fig. 3A). To investigate these events further, DNA–M/R complexes were imaged using FS-AFM in fluid and the binding activity was observed over ~30 min. DNA was deposited on a mica surface functionalized with aminopropyl silatrane (APS) which enables the attachment of negatively charged DNA via its positively charged amino groups in the pH range of stable DNA duplexes (35). Three examples of movies (Movies S1–S3) and representative image sequences (Figs. 4A and 5 and *SI Appendix*, Fig. S4) are presented.

In the first example (Movie S1 and Fig. 4A), we observed Rad50 coiled coils extending from the globular core of an oligomeric M/R assembly interacting with the dsDNA (Fig. 4A, red circles). The contact points with the DNA substrate shifted throughout the observation time, indicating a dynamic interaction during which several different coiled coils connected with and dissociated from the substrate. The coiled-coil apices seemingly bind and disengage from the double helix, alternating between the two conditions along the dsDNA template (Movie S1). Furthermore, in the first 24 min, the DNA template seems to be physically displaced (as exemplified by the movement of the DNA template toward the right of the frame in Movie S1). In this example, at the timepoint 24:30 (minutes:seconds) a second, larger M/R aggregate became attached to the mica close to the dsDNA. Upon arrival, the coiled-coil apices of this second M/R complex also interacted with the DNA template (Fig. 4A, blue circles). These coiled-coil apices also seemed to exert a pulling force upon the dsDNA substrate, physically shifting it at two disparate points of interaction; the first of these interaction sites was eventually released at 25:30 min (Fig. 4A). The second contact point of a different Rad50 coiled coil, which associated

with the dsDNA free end, remained uninterrupted throughout the remainder of the observed period (Fig. 4A, timepoints 25:00 to 29:00, blue circle).

To further assess and quantify the interaction sites between the Rad50 coiled coil and the dsDNA molecule, we measured the height of the dsDNA substrate alone, that of the Rad50 coiled coils in the absence of DNA, and that of dsDNA at points of interaction with the Rad50 coiled coil during the scan of Movie S1 (as presented in *SI Appendix*, Fig. S3). The resulting graph is shown in Fig. 4B. The height of the DNA at the point of contact with the coiled-coil apices of Rad50 (Fig. 4A, red circles) changed over time in an "oscillating" binding pattern. The lowest height in this oscillation corresponded to the height of the dsDNA substrate alone, and the greatest height corresponds to the sum of the mean height of the dsDNA substrate plus the mean height of Rad50 coiled coils (Fig. 4B, details in legend). This pattern indicates transient interactions between the Rad50 apices and the DNA substrate and accords with the interpretation of the binding and disengaging movement along the dsDNA template described above.

Movie S2 together with the corresponding Fig. 5 illustrates a further example of DNA template translocation on the mica due to association with the M/R protein complexes via the Rad50 coiled-coils apices. Here, we observed the arrival of an M/R oligomer that appears to bind the dsDNA substrate via canonical associations at the globular domains, although notably a second attachment is made via the coiled-coil regions forming a DNA loop (Fig. 5, red circles). These binding events resulted in a marked translocation of the DNA substrate across the mica substrate despite the APS attachment, suggestive that mechanical forces generated by the M/R complex are involved. Further dramatic movements of the DNA substrate were observed coincident with the arrival of additional M/R oligomers (e.g., at 6:00 min and 24:30 min). In all examples the Rad50 coiled coils again perform a binding and disengaging action, shifting the DNA duplex in different directions within the observed area over the time course of 30 min.

In the third example (Movie S3 and the corresponding image sequence in *SI Appendix*, Fig. S4), the free DNA ends of the linear (5.4 kb) dsDNA were repositioned by the M/R oligomeric complexes, and again transient DNA associations with the Rad50 coiled-coil apices appeared to be involved in these movements. In this example it was particularly evident that one of the ends of the DNA substrate (colored in red in *SI Appendix*, Fig. S4) was immediately repositioned toward the left side of the observation frame on arrival of a first M/R oligomer (10:00, *SI Appendix*, Fig. S4) but in contrast was then rapidly translocated back toward the right of the frame following the arrival of two additional M/R oligomers (time 10:30, *SI Appendix*, Fig. S4). Throughout the remainder of the observation time, this end of the DNA substrate was then translocated stepwise back toward the left side of the observation frame, again through binding and disengaging, as observed in the other examples.

The other free DNA end (colored blue in *SI Appendix*, Fig. S4) underwent less pronounced movements, but at 18:00 a portion of this section of the DNA formed a loop which was drawn left toward the newly arrived M/R oligomers via association with the coiled-coil apices (top right edge of blue box, *SI Appendix*, Fig. S4). We noted that following the arrival of the first M/R oligomer at 10:00, there was at least one stable DNA–protein contact point, likely via the globular domains of the complex (orange region, *SI Appendix*, Fig. S4), at which the DNA remained throughout the whole imaging time. However, in contrast, transient and dynamic DNA binding was observed in general between the M/R complexes and the substrate, which involved DNA interactions via the Rad50 coiled-coil apices.

In order to quantify the increased movements of the DNA substrate via this transient binding by the M/R protein complex
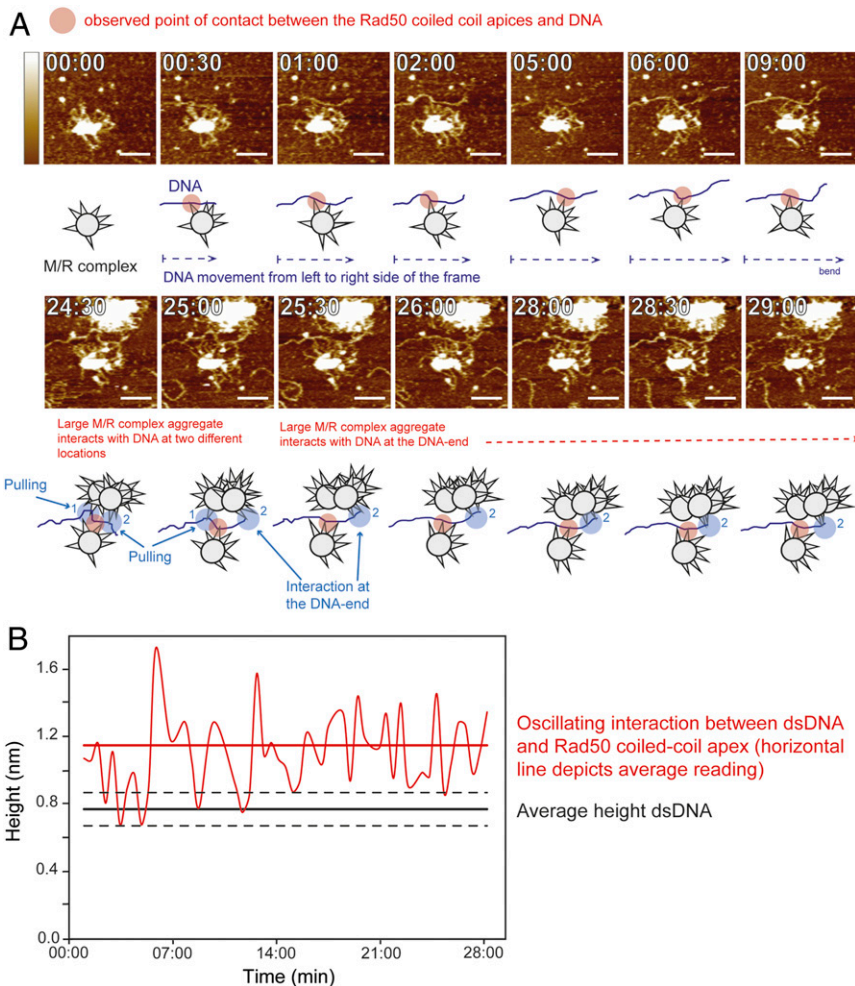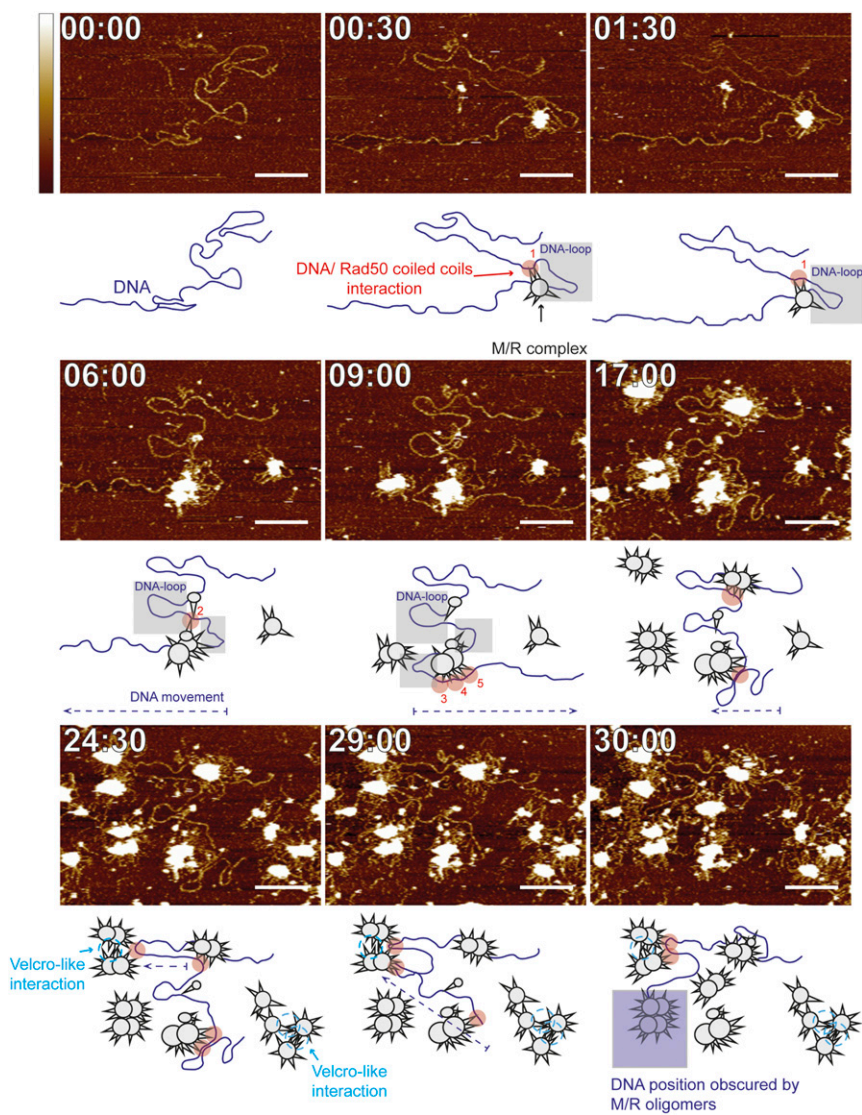
Fig. 4. Real-time FS-AFM imaging of DNA binding and translocation following association with the Rad50 coiled-coil apices of the wild-type M/R complex (example 1). (*A*) Selected images from Movie S1 captured in fluid over 29 min (00:00 to 29:00). The wild-type M/R interacts with the DNA substrate via the Rad50 coiled-coil apices. Following the initial interaction with the DNA duplex (00:30), sustained contact via the Rad50 coiled coils is observed in subsequent frames (cartoons below, red-shaded circles). Examination of individual Rad50 apices reveals a pattern of alternate binding and disengagement from the DNA substrate resulting in the intermittent movement displacing the DNA strand (also see *B* and Movie S1) from *Left* to *Right* (cartoons, blue dotted arrows). A second M/R protein oligomer arrives at the observed area (24:30) and binds to another region of the DNA strand via the ends of Rad50 coiled coils making two different contact points (cartoons: blue shaded circles, 1 and 2). This Interaction causes a transient pulling of the DNA substrate toward the newly arrived protein complex at the first contact point (blue-shaded circle, 1) (24:30 to 25:00). Although this DNA–coiled coil interaction site is eventually released (25:30), the DNA molecule stays tethered to the second M/R aggregate via the other contact point (the DNA end is eventually stably bound at this point: 25:30 to 29:00, blue-shaded circle, 2). Time in minutes and seconds. (Scale bar: 50 nm.) (Height scale bar: 2 nm [dark to light].) (*B*) Measurements of the height of the DNA molecule at the observed point of contact with the coiled-coil apices of Rad50 in Movie S1 (*A*, red-shaded circles) reveal an oscillating pattern of interaction. The lowest points of the oscillation are similar to the height of the dsDNA alone (0.77 ± 0.10 nm, horizontal black lines), the highest peaks of the oscillation occur at 1.1 ± 0.20 nm (horizontal red line), a value corresponding to the sum of the average height of the dsDNA plus the average height of a Rad50 coiled coil (0.57 ± 0.13 nm, not shown). The periodic height variation indicates alternate engagement and disengagement of the Rad50 apices from the double-helix substrate.

during FS-AFM imaging in fluid conditions, and to control for DNA movement in the absence of protein, the contour of the DNA duplex (5.4 kb) on the APS mica surface was tracked before and after addition of the protein sample in two independent examples (*SI Appendix*, Fig. S5). The DNA contours were captured in 30-s intervals. In examples without the M/R complex, the *x,y* coordinate position of the DNA substrate on the mica surface moved minimally. In clear contrast, the DNA substrate dramatically shifted position on the mica surface upon addition of the complex and continued to be moved throughout the observed period (*SI Appendix*, Fig. S5 *A* and *B*). However, this increased movement of DNA is only observed if the protein molecules attach to the mica close enough to interact with DNA via the coiled coils. If the M/R complexes land too far away from the DNA (as seen in Movie S4), no significant movement of DNA molecule is observed.

It is noteworthy that in these FS-AFM analyses in fluid, individual M/R complexes also interact with each other via the canonical intermolecular association of their Rad50 coiled-coil ends. We observed that the extended Rad50 zinc hooks of the winged M/R conformations could associate with M/R ring arrangements, in a manner reminiscent of the "loops" and "hooks" in "Velcro-like" fastenings (aquamarine circles, Fig. 5). Similar binding interactions have been observed with human M/R intercomplexes, which also associate via Rad50 zinc hooks (34), although our FS-AFM analyses reveal that these associations can be extremely transient and dynamic.

Molecular Dynamics Simulation and Electrophoretic Mobility-Shift Assays. A classical MD method was used to further investigate the interactions observed with AFM imaging between the Rad50 coiled-coil apex and a dsDNA blunt-ended molecule (*SI Appendix*, Fig. S6A). The aim of this was to identify structural aspects of the interaction between the apex of a wild-type Rad50 monomer encompassing the central zinc-hook motif, (modeled using the *Pyrococcus furiosus* Rad50 crystal structure; Protein Data Bank [PDB]:1L8D) (36) and a 20-mer piece of simulated dsDNA. From five 100-ns simulations, the orientation of the Rad50 relative to the dsDNA was examined. These simulations showed that the modeled Rad50 zinc-hook head should be capable of tracking along the minor groove of DNA until the DNA end is encountered, thereby providing one plausible mechanism for facilitating the increased localization of wild-type M/R to DNA ends (*SI Appendix*, Fig. S6A and Fig. 2). The modeling was also consistent with a positively charged zinc ion (held by the cysteine residues at the zinc hook) interacting with the negatively charged sugar-phosphate backbone of the DNA via Coulombic interactions (*SI Appendix*, Fig. S6A). Taken together, the findings of the molecular dynamics modeling are consistent with the mode of binding observed with AFM.

In order to confirm the interaction between the coiled-coil regions abutting the zinc-hook region and DNA, we generated a construct (Zn231) which is representative of a 230-amino acid coiled-coil region including the centrally located CXXC zinc hook. We demonstrated by electrophoretic mobility-shift assay

Fig. 5. Large-scale translocation of DNA substrates following association with the Rad50 coiled-coil apices of the wild-type M/R complex. Representative images from Movie S2 captured in fluid over 30 min. Wild-type Mre11/Rad50 (M/R) oligomer interactions with the DNA substrate via the Rad50 coiled-coil apices indicated by red-shaded circle cartoons. Blue dotted arrows indicate direction of DNA movements. The first M/R protein complex to arrive (00:30) associates via both the globular domains and the coiled coils, and the interaction with the coiled-coil apices (red circle 1, 00:30) stabilizes a large loop (gray-shaded region) of DNA which is displaced toward the left of the frame. Upon arrival of another large M/R oligomer, the first M/R complex dissociates with the substrate and the looped region of the DNA becomes compressed into two new loops (06:00, gray-shaded region). The new loops are stabilized by coiled-coil connections, which extend from the newly arrived oligomer, and from a smaller M/R complex in the center of the frame that had arrived earlier (red circle 2). At 09:00 new contacts with the M/R coiled coils (three overlapping red circles 3, 4, and 5) associate with the opposite end of the DNA molecule (which had previously remained in a horizontal and almost static position) repositioning this end of the molecule from the left-hand side to the right-hand side of the frame, forming a third loop. In the following frames (17:00 to 30:00) more M/R oligomers land close to the DNA template and intermittent binding movement of the Rad50 coiled coils results in a net movement of the DNA substrate toward the top left of the frame (30:00). Aquamarine circles in the enlarged frame highlight interactions between the M/R molecules. Velcro-like associations between the coiled-coil regions also appear to hook M/R oligomeric complexes together. Time appears in minutes and seconds. (Scale bar: 100 nm.) (Height scale bar: 1.5 nm [dark to light].)

(EMSA) that this region of Rad50 is able to bind to a 400-bp DNA substrate and we approximated the K_D of this association at about 4 μM (see *SI Appendix*, Fig. S7 for further details).

AFM Visualization of ATP-Dependent DNA Strand Separation Mediated by Mre11/Rad50 Complexes. We found direct evidence of DNA strand separation by *S. acidocaldarius* M/R proteins as a result of ATP hydrolysis. When wild-type *S. acidocaldarius* M/R proteins were incubated with linear dsDNA substrates in the presence of 3 mM ATP at the physiological temperature of 60 °C and visualized by AFM in dry conditions, DNA strand separation, extending for several hundred base pairs, was observed at both DNA ends and, unexpectedly, at internal sites on the DNA. Critically, these events occurred exclusively in the presence of ATP, and this unwinding activity was not observed in the presence of AMP-PNP (Fig. 6 *A* and *B* and *SI Appendix*, Figs. S8 and S9). To differentiate between separated single strands (ss) and intact DNA double helices, we measured the height of DNA captured during imaging, as shown in Fig. 6*C*. The height of the unwound ssDNA regions was approximately half the height of dsDNA regions (Fig. 6*D*; details in legend).

Although subtle DNA unwinding effects at DNA ends have been reported in studies of the M/R complex from other species

(37–39), the degree of strand separation mediated by the *S. acidocaldarius* Rad50 complex was striking and unprecedented. Our AFM analyses revealed that, following the DNA strand separation by the *S. acidocaldarius* complex, the M/R proteins remained attached at the boundaries of the unwound part of the dsDNA, which had opened into broad, single-stranded "bubbles" (Fig. 6*A* and *SI Appendix*, Fig. S8). In the presence of AMP-PNP, the wild-type M/R complex was also bound to the DNA duplex, but negligible unwinding activity was observed (Fig. 6*B* and *SI Appendix*, Fig. S9*B*).

We confirmed that DNA unwinding by the *S. acidocaldarius* complex is ATP dependent by use of catalytically inactivated mutant protein, the Rad50 Walker-A box ATPase mutant (K36A). Notably, however, unwinding was still observed when a Mre11 nuclease domain mutant (H85S), a control mutation that should not affect the ATPase activity of the M/R complex, was used in these assays (Fig. 6*E* and *SI Appendix*, Figs. S9*C* and S10). Furthermore, buffer-only controls (no protein) were also performed to confirm that the strand separation was due to the ATP-dependent activity of the complex and not due to thermal fraying of the DNA strands at high temperature (60 °C) (Fig. 6*E* and *SI Appendix*, Fig. S9*A*).

In the absence of the complex, strand-separation events in the 5.4-kb linear dsDNA substrate ($n = 700$) were minimal ($1.64 \pm 0.96\%$).

Fig. 6. ATP-dependent DNA unwinding by Mre11/Rad50. (*A*) DNA unwinding by Mre11/Rad50 complex (M/R) in the presence of 3 mM ATP. Blue arrows indicate the unwound part of the dsDNA; black arrows indicate M/R complexes bound at end boundaries of the unwound dsDNA regions; red arrows show the intact double helix. (*B*) DNA unwinding by the wild-type M/R is negligible in the presence of AMP-PNP. M/R complexes (black arrows) are bound to dsDNA, but no unwinding events can be identified. (Scale bar: 100 nm in *A* and *B*). (Height scale bar: 2 nm [dark to light].) (*C*) Representative image of the separated DNA single strands (blue line) and intact double strands (red line) (*Left*) and corresponding cross-sections (*Right*). (Scale bar: 50 nm.) (Height scale: 2 nm [dark to light].) (*D*) Height distribution of DNA molecules (*n* = 100) in a sample with partly unwound DNA molecules displays peaks at 203 ± 13 pm (*P* < 0.0001) and 414 ± 13 pm (*P* < 0.0001). The two peaks represent the unwound (single-stranded) and double-stranded DNA regions, respectively. (*E*) Quantification of the DNA unwinding events (*n* = 700 per experimental condition). When 3 mM ATP was included in the reactions 20.22 ± 7.61% or 24.17 ± 8.84% of the DNA molecules were partly unwound in the presence of the wild-type M/R or the H85S mutant, respectively. In the presence of the nonhydrolyzable ATP analog (AMP-PNP) this percentage of unwound DNA molecules was negligible. Only 2.87 ± 0.54% of the strands were partly unwound when the K36A (Walker A) mutant was tested in the presence of 3 mM ATP. Error bars represent SEM.
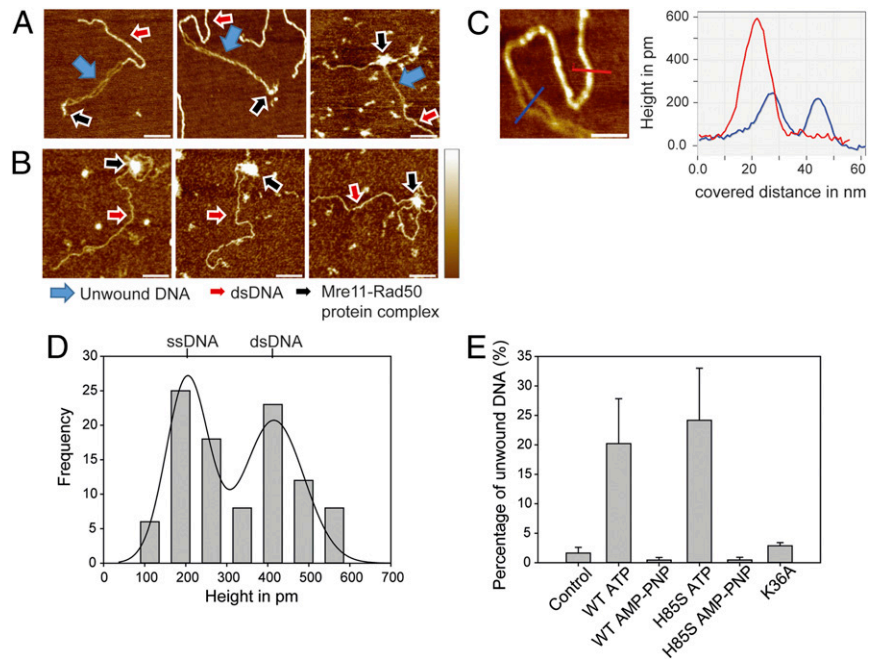
As expected, mutation of the Mre11 nuclease active site residue H85 did not affect strand separation by the M/R tetramer, and ATP-dependent DNA unwinding activity of this complex was similar to that of its wild-type counterpart (*SI Appendix*, Fig. S10). Over 20% of the DNA double helices (*n* = 700 per group) were partially unwound in the presence of either the wild-type complex or the H85S mutant complex. The activity in both cases was ATP dependent: in the presence of AMP-PNP, DNA unwinding was negligible whether the wild-type complex or the H85S mutant complex was used (Fig. 6*E*).

In strong contrast to the result with the H85S mutant, the mutation of the conserved Mre11/Rad50 Walker-A lysine to alanine (K36A; a residue essential for ATP hydrolysis) inhibited ATP-dependent DNA strand separation (Fig. 6*E* and *SI Appendix*, Fig. S9*C*). Only 2.87 ± 0.54% of DNA strands were partially unwound when the Mre11/Rad50 Walker-A ATPase mutant K36A mutant complex was used in the presence of ATP, a proportion similar to that observed in the presence of the active complex and AMP-PNP. This result confirms that Rad50-dependent ATP hydrolysis is essential for the DNA unwinding activity of the wild-type M/R protein complex. Such extensive DNA unwinding activity by the archaeal complex, particularly at internal locations far removed from the DNA ends, has not been reported to date and is an intriguing discovery regarding the ability of the system to manipulate nucleic acid templates. It is noteworthy that the described DNA unwinding is only evident during experimental conditions at 60 °C when the temperature permits action by the thermophilic *S. acidocaldarius* M/R complex. In contrast, negligible unwinding was detected in the presence of ATP at 45 °C and lower temperatures (37 °C and 25 °C) (*SI Appendix*, Table S4).

In order to assess the stoichiometry of the M/R complex at the unwound DNA regions we performed a volume analysis (*SI Appendix*, Fig. S2*B* and Note S2) to quantify the number of wild-type complexes attached at the boundaries of the unwound part of linear dsDNA as shown in Fig. 6*A* and *SI Appendix*, Fig. S8. M/R complexes measured at the boundaries of unwound DNA peak at two extremes, single heterotetramers (1t) and large

oligomers (>8). This result indicates that DNA unwinding can be executed by a single M/R tetramer, while by contrast DNA binding and tethering require multiple copies of M/R (*SI Appendix*, Note S2).

To further investigate the substantial unwinding events by M/R, we also performed the corresponding reactions in an ensemble biochemical assay where S1 nuclease is added after a preincubation with the M/R proteins on a linear dsDNA substrate. Commercial *Aspergillus* S1 nuclease is suitable for these reactions as this nuclease retains activity at 60 °C (40). As shown in *SI Appendix*, Fig. S11, these assays reveal that the S1 nuclease displays more activity in the presence of the M/R protein complex, but critically only in the presence of ATP. We infer that the unwound single strands clearly observable by AFM are more amenable to processing by the S1 nuclease, which displays a preference for single-stranded substrates.

Discussion

Structural Analyses of the *S. acidocaldarius* Mre11/Rad50 Complex. AFM imaging in fluid conditions demonstrated that *S. acidocaldarius* M/R complexes predominantly exist as four different architectural arrangements—namely, ring, winged, dumbbell, and half-dumbbell. These four conformations (of which the ring was the most frequently observed) have been identified before in different model systems, including bacteria, archaea, yeast, and mammalian cells (12, 28, 34, 41–43). In this previous work (41), dumbbell and half-dumbbell arrangements were the most frequently observed forms in bacterial systems, whereas the winged and ring forms were primarily detected in archaeal, human, and yeast complexes of M/R homologs (12, 28, 34, 43) (*SI Appendix*, Table S3 and Note S1).

The measured lengths of single *S. acidocaldarius* Rad50 coiled-coil regions and of dimerized coiled coils closely corresponded to the theoretical lengths (Fig. 1*B*). The intermolecular distance between DNA strands bridged by archaeal Rad50 molecules (~670 Å for *S. acidocaldarius* and ~600 Å for *Pyrococcus furiosus*) is somewhat shorter than that seen with the eukaryotic homologs (~1,200 Å) but is notably longer than bacterial analogs such as the

bacterial SMC superfamily proteins *Escherichia coli* MukB (~490 Å) or *Bacillus subtilis* BsSMC (~410 Å) (12, 24, 28, 41, 44, 45) (Fig. 1*C*).

DNA Binding by the Rad50 Coiled-Coil Regions. In our study of the *S. acidocaldarius* M/R complex, we observed initially that the complex interacted with DNA canonically via its catalytic globular head domains, as reported previously (12, 15, 30, 39, 46–48) (Fig. 2). In these cases, the complex bound to either the DNA ends or internal regions away from the ends of the DNA duplex, although we observed a significant preference for the DNA-end binding by the WT complex. In some instances, the wild-type heterotetrameric complex seemed to form oligomers to join two DNA ends, presumably via Rad50 zinc-hook-mediated dimers (17, 33, 49); alternatively, it remains plausible that the globular DNA-binding regions of the Mre11 dimer could play a role in this bridging, as has been reported previously (13, 34, 50). By contrast, DNA-end tethering was not detected when the MR(Δcc) mutant complex was used instead of the wild-type complex. These observations indicate that the full-length Rad50 coiled coils are essential for DNA tethering, supporting the canonical view that tethering between two DNA ends occurs predominantly via intermolecular association of the M/R complexes via the Rad50 zinc hooks. However, we also observed unexpected direct interactions between these coiled-coil regions and the DNA substrates. Interestingly, the DNA-binding profile of MR(Δcc) was also notably different from that of the wild-type complex, as no significant preference for binding to the free DNA ends was observed (Fig. 2 *B, i–iii* and Fig. 2*C* and *SI Appendix,* Note S3).

These results indicate that the *S. acidocaldarius* Rad50 coiled-coil domains have a role in locating the protein complex at the DNA ends. Interestingly, the human M/R mutant equivalent to MR(Δcc) fails to associate with DNA (51), while an isolated full-length human Rad50 coiled-coil region exhibited putative DNA-binding activity in vitro, suggesting that the coils act not only as bridges between disparate Rad50 globular domains but also actively participate in association with DNA substrates (51). This binding has not been observed previously in the context of the whole M/R complex, and in support of that hypothesis, we have now provided direct visualization of DNA interactions via the Rad50 coiled coils of the *S. acidocaldarius* M/R complex.

Transient interactions were observed between the DNA substrate and the highly conserved Rad50 coiled-coil regions near the zinc-hook apex of Rad50. While DNA interactions at the analogous hinge domains of other SMC superfamily proteins have been reported previously (25, 26), the zinc-hook regions in Rad50 have until now only been proposed to function in protein–protein interactions rather than in protein–nucleic acid associations. Following our observation in dry imaging conditions, that the Rad50 coiled-coil domain interacted with DNA molecules (Fig. 3), we set out to observe the DNA-binding activity of the *S. acidocaldarius* M/R complex in near real-time by FS-AFM imaging in fluid. We observed dynamic interactions of the Rad50 apices with the DNA substrate, during which the complex seemed to be capable of displacing DNA molecules despite their firm attachment to an APS-modified mica surface (Figs. 4*A* and 5, *SI Appendix,* Figs. S4 and S5, and Movies S1–S4). On the basis that repositioning of DNA ceased as soon as the Rad50 coiled-coil apices recognized the DNA end (Fig. 4*A*), we propose that the complex uses this activity to traverse the DNA substrate until a terminus is reached. The height analyses at the points of contact between the DNA molecule and Rad50 coiled coils in Fig. 4*B* support a transient binding action consistent with a repetitive binding and disengaging process of the Rad50 coiled coils on the DNA. This process is likely responsible for the increased movement of DNA in the presence of M/R when compared with the limited DNA rearrangements observed in the

absence of the complex (see *SI Appendix,* Note S4 and Fig. S5 for further analyses).

We also applied molecular dynamics simulations to further investigate the Rad50–DNA interaction observed. Our simulation, based on a *P. furiosus* Rad50 coiled-coil monomer crystal structure (PDB:1L8D) that is equivalent to the zinc-hook and coiled-coil regions of the *S. acidocaldarius* complex, suggested that this mode of interaction might permit sliding of the region that contains the Rad50 hook along the minor groove of the DNA duplex until the DNA end is encountered (*SI Appendix,* Fig. S6). More complex simulations of the Rad50 coiled-coil dimer will be needed to verify this observation. Nevertheless, our FS-AFM analyses reveal that, although the complex seems able to bind to any point along the length of linear dsDNA substrates, most DNA-binding events occur at the DNA ends. Furthermore, our EMSA work demonstrated that the *S. acidocaldarius* Rad50 coiled coils alone exhibit DNA-binding activity (*SI Appendix,* Fig. S7), consistent with the suggestion that the coiled-coil regions are important for DNA binding in human Rad50 counterparts (51).

These data suggest that the M/R complex uses the Rad50 coiled-coil domains around the central zinc-hook motif to facilitate its traversal of a DNA duplex to deposit the archaeal complex at DSB damage sites. Our observations complement and extend a recently published M/R sliding model (32), in which the human M/R assembly (which in eukaryotes forms a tripartite M/R/N complex with a third protein, Nbs1/Xrs2) is capable of translocating along chromatin-bound DNA via the globular Rad50 nucleotide binding site until a DNA terminus is encountered. The study revealed that the human M/R/N complex can travel by facilitated diffusion from internal locations on DNA molecules to the DNA ends, even on substrates that are wrapped around nucleosomes. Critically, truncation of the Rad50 coiled coils significantly reduced the ability of the human M/R/Nbs1 complex to bypass the nucleosomes, and this truncated complex was more prone to dissociation from the DNA substrate (32). Rather than exclusively using the globular domains of M/R as suggested in that study, we propose that the transient DNA–protein interactions with the coiled coils around the Rad50 zinc-hook regions assist complex binding and movement along DNA strands. Indeed, we suggest that transient interactions with the coiled coils abutting the zinc-hook region ensure that the complex remains associated with the DNA molecule during facilitated diffusion. Furthermore, the dramatic displacement of the DNA substrates observed in our FS-AFM videos is indicative of a more active mode of substrate translocation.

Previous studies have demonstrated that structural variations in the M/R globular domains resulting from DNA binding or nucleotide hydrolysis are intrinsically linked to changes in the architecture of the coiled coils and hooks (24, 28–30). Conversely, interactions at the zinc hook can transmit information back along the coiled coils to influence the globular catalytic domains (11, 30). This allosteric regulation is presumably central to the coordination of chromosome tethering and DNA end-resection functions of the M/R complex during repair. Based on the DNA tethering by the *S. acidocaldarius* coiled-coil regions near the zinc-hook apices observed in our current study, we suggest that this allosteric regulation could permit the Rad50 coiled coils to communicate their positioning upon binding a DNA template and trigger additional long-range DNA-binding events at the globular catalytic head as soon as the DSB is detected.

Visualization of ATP-Dependent DNA Unwinding by Mre11/Rad50. Our other striking finding was that the *S. acidocaldarius* M/R complex was capable of driving a marked and ATP-dependent strand separation of the dsDNA substrate. Less extensive ATP-dependent DNA unwinding events limited to DNA ends have been reported in studies of other M/R complexes (17, 37–39). However, our observations are an example of M/R-mediated

strand-separation across several hundred base pairs. Crucially, we frequently observed unwinding at internal regions of the substrates and not only at the DNA ends. The fact that the separated ssDNA strands did not reanneal without additional stabilization by DNA-binding proteins such as SSB or the RadA recombinase suggests that the unwound DNA was stabilized by the physical interaction with the nickel-modified mica surface. In addition, our rapid deposition of the M/R–DNA samples on the mica surface likely inhibited annealing of the ssDNA strands, allowing the capture and visualization of these events. This has been seen in the past in the context of nanobubbles by Adamcik et al. (52). Volume measurements of complexes at the boundaries of unwound DNA indicate that DNA unwinding can be executed by a single M/R tetramer, while DNA-end binding and tethering (as in Fig. 2A) require multiple copies of M/R (*SI Appendix*, Fig. S2 and Note S2).
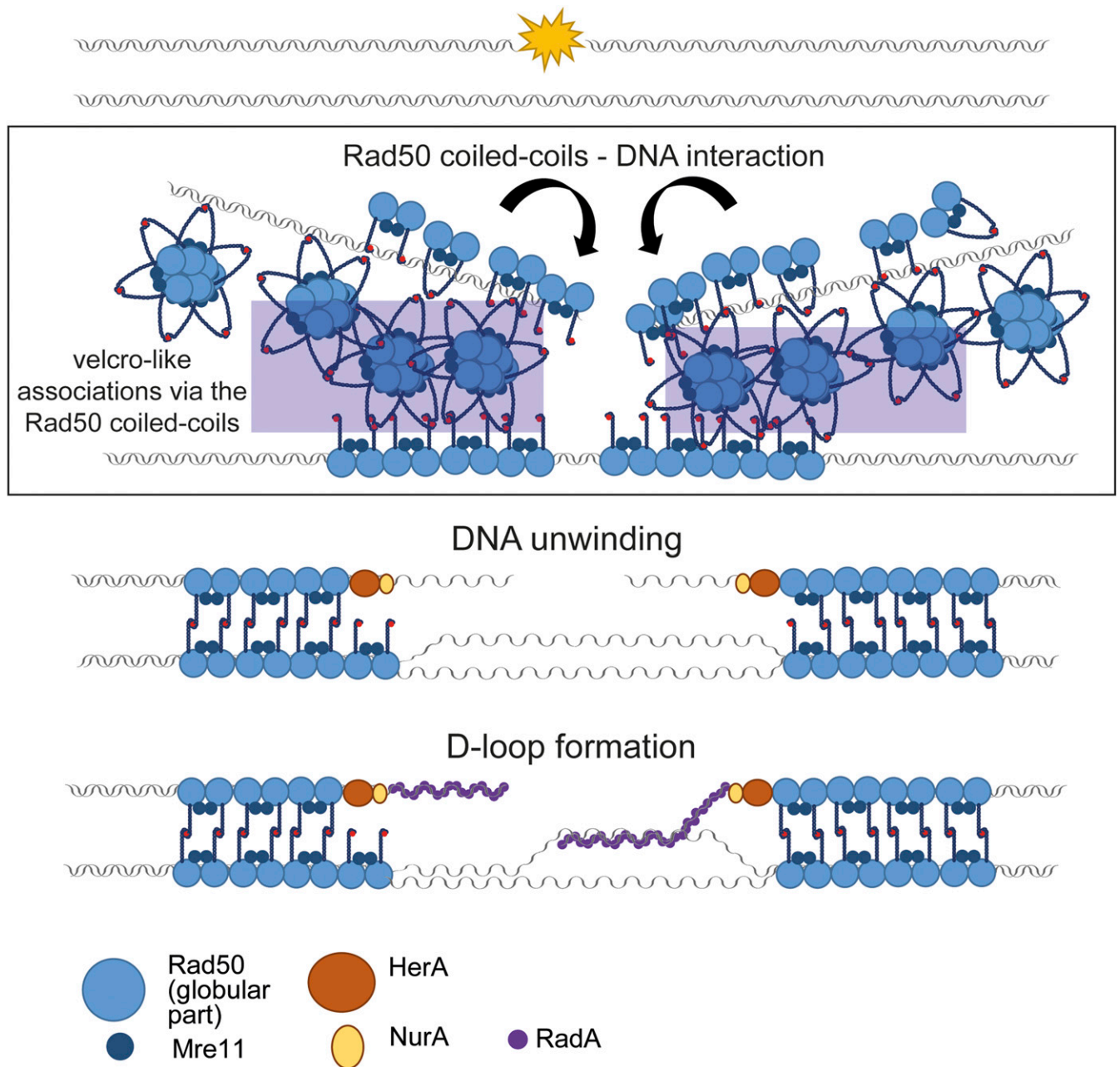
Fig. 7. Proposed modes of action of the *S. acidocaldarius* Mre11/Rad50 (M/R) complex on DNA to mediate chromosomal pairing and speculative involvement of the M/R unwinding activity during HR-mediated DNA DSB repair. The M/R protein complexes scan the DNA double helix and slide toward a double-strand break, facilitated by associations with the Rad50 coiled coils. Engagement of the nucleotide binding domains of the Rad50 globular head on the DNA substrate results in dramatic conformational changes in the Rad50 coiled coils, switching from the ring-shaped conformations (connected intramolecularly at the zinc hooks) to rigid open coiled-coil conformations (30). Associations with the homologous chromosome are then formed via Velcro-like interchromosomal connections between the Rad50 zinc hooks and coiled-coiled regions (blue-shaded region). We propose that M/R oligomers may also link the broken DNA termini while the homologous chromosome remains held in proximity by Rad50 intermolecular associations. Consistent with previous studies, the HerA–NurA DNA end-resection machinery (1, 61, 62) generates long-range 3′ ss-DNA overhangs. We speculate that the intrinsic unwinding activity of the M/R complex may open the DNA duplex on the homologous chromosome to facilitate D-loop formation and strand invasion by the RadA proteofilament, although this hypothesis requires experimental verification.

The M/R complex has well-established roles in the various stages of DSB break repair, from DNA end recognition to the facilitation of single-stranded resection required for the strand invasion and the subsequent homology search by the RecA/RadA/Rad51 nucleoprotein filaments (7, 53–55). We suggest that if the extensive DNA strand separation by the archaeal complex observed in this study can be targeted to a region on a homologous chromosome equivalent to the site of DNA damage, then M/R might also aid the homology search and strand-invasion events by opening the DNA duplex on the homologous chromosome. Previous studies have shown that strand invasion by RecA/RadA/Rad51 nucleoprotein filaments is significantly stimulated by ATP-dependent unpairing of the homologous DNA duplex (56–59), but this function has been attributed to the archaeal/eukaryotic Rad54 protein. Studies of eukaryotic Rad54 have shown that it uses its dsDNA-dependent ATPase activity to translocate along the DNA molecule and topologically unwind dsDNA (56–59). This Rad54 dsDNA unwinding activity is crucial for strand invasion of the nucleofilament (56, 58, 59). In addition, a recent in vitro study (60) demonstrated that the bacterial SMC-like protein RecN significantly enhances RecA-mediated strand invasion and D-loop formation as a result of its ATP hydrolysis, possibly by powering translocation along the target DNA. Whether the M/R complexes use similar ATP-dependent mechanisms to unwind or translocate along DNA requires further investigation, but these putative modes of action seem compatible with our current analyses of the *S. acidocaldarius* M/R complex, where pronounced repositioning and extensive unwinding of DNA substrates were apparent.

Our observations of the *S. acidocaldarius* complex upon interaction with DNA substrates and of the macromolecular architectural changes that occur during these binding events have led us to propose a putative model for M/R functions during recombinational DSB break repair in archaea (Fig. 7). In this model, several M/R molecules bind to and move along the DNA duplex, searching for the broken terminals and using the globular nucleotide binding site as suggested by Myler (32), stabilized by the transient interactions with the Rad50 coiled coils and zinc-hook regions observed in our study. Higher-order M/R assemblies can then bring the termini of a DSB into close proximity by M/R dimer formation or *Velcro*-like coupling between ring and winged M/R forms as observed in this study (Fig. 5). Following the long-range DNA-end resection of the DSB by the archaeal HerA/NurA complex (61, 62) (or the analogous machinery in eukaryotic systems) (63) the M/R complexes may then unwind the equivalent DNA sequence on the homologous chromosome. This unwinding would facilitate the homology search and strand invasion of the RadA proteofilament on the homologous template. We suggest that identification of the dsDNA break by the zinc-hook region of Rad50 might also subsequently transmit allosteric changes to the globular domains of the complex via the Rad50 coiled coils to facilitate the unwinding of the appropriate region on the homologous chromosome. Further single-molecule studies will be required to test this model and verify how the M/R–DNA interactions operate alongside other DNA-repair machineries that are involved in the DNA end-resection processing steps, and in the downstream strand-invasion steps of HR.

By applying recent advances in AFM-based high-resolution visualization techniques in fluid to examine the M/R complex from the thermophilic archaeon *S. acidocaldarius*, we have gained insights into how this enigmatic DNA-repair complex might mediate DNA DSB repair. Further studies are needed to complete the picture of how the Mre11 nuclease and the Rad50 SMC superfamily ATPase work together to facilitate the downstream homology search and strand-invasion steps in the HR-repair pathway. These would no doubt be instrumental in the elucidation of the complex and dynamic conformational changes that are central to the operation of this intriguing DNA-repair machinery.

Methods and Materials

Expression Constructs and Protein Purification. *S. acidocaldarius* Mre11 and Rad50 open reading frames (ORFs) were cloned into pET28a and pETDUET expression vectors, respectively. All proteins and protein complexes were expressed in *E. coli* Rosetta (DE3) pLysS (Novagen) competent cells; the Mre11/Rad50 constructs were cotransformed as a pair. His-tagged proteins were purified by Nickel-NTA immobilized metal affinity chromatography, treated with Benzonase Nuclease (Merck Millipore) and run over a Superdex 200 16/60 (GE Biosciences) size-exclusion column. Full details of the cloning and protein expression, including details of the site-directed mutagenesis, are given in *SI Appendix*.

SEC-MALS Analyses of the Oligomeric Forms of the Mre11/Rad50 Complex. For SEC-MALS analyses 100 μL protein complex at 2 mg·ml^{-1} was passed over a Superdex 200 10/300 Increase GL column (GE Healthcare). The column output was fed into a DAWN HELEOS II MALS, followed by an Optilab T-rEX differential refractometer (Wyatt Technology); full methodology is provided in *SI Appendix*.

Protein Sample Preparation and AFM Imaging in Fluid. The wild-type M/R complex was imaged in fluid conditions on APS mica (64). APS (35) was provided by Yuri L. Lyubchenko, University of Nebraska Medical Center, Omaha, NE. For the mica functionalization, 60 μL of 167 μM APS solution was applied onto a freshly cleaved mica sheet, incubated for 30 min, washed three to four times with 1 mL BPC (BioPerformance Certified) water (Sigma-Aldrich), and dried under nitrogen gas. The frozen protein aliquots were thawed at room temperature and heated at 60 °C for 10 min. Then, 6 nM M/R complex in buffer (50 mM potassium acetate, 20 mM Tris-acetate, pH 8, 10 mM magnesium acetate, 150 mM NaCl) was applied on the dried APS-modified mica surface and incubated for 10 min. After washing the mica three times with the same buffer, a droplet (∼200 μL) of buffer was left on the mica surface for fluid AFM imaging.

Protein Volume Analysis. For the volume measurement of the wild-type *S. acidocaldarius* Mre11/Rad50 complex (*SI Appendix*, Table S1), only the volume of the globular protein part was considered, signifying that the threshold for the corresponding sample was set at a height that would guarantee that the globular part is fully measured, but the volume of the tails is not taken into account, as previously described (65). The volume distribution was summarized in a bar chart with a bin range which was chosen in accordance with how many Mre11/Rad50 heterotetramers (1d, 1t–8t) can be accommodated per bin volume. The bin range begins from the volume of a dimer (1d; Mre11 monomer associated with one globular Rad50 ATPase domain), up to a multiple of eight Mre11/Rad50 tetramers (8t).

DNA Substrates. Linear 5.4-kb and 3-kb dsDNA substrates were prepared by PCR with the PhiX virion DNA serving as templates, respectively.

Linear dsDNA Binding by Wild-Type Mre11/Rad50 and MR(Δcc) Mutant. Totals of 0.2 nM of 5.4 kb linear dsDNA and 6.5 nM of the wild-type M/R, or 0.2 nM of 3 kb linear dsDNA and 6.5 nM of the MR(Δcc) mutant were incubated at 60 °C for 15 min in reaction buffer (50 mM potassium acetate, 20 mM Tris-acetate, 10 mM magnesium acetate, 150 mM NaCl, 0.05 mM zinc chloride, adjusted to pH 8, using a 1 M potassium hydroxide solution) in the presence or absence of 3 mM ATP or nonhydrolyzable ATP or AMP-PNP before being prepared for AFM imaging in air on nickel-modified mica (see below).

Determination of the DNA-Binding Location of the Wild-Type Mre11/Rad50 and MR(Δcc) Mutant on Linear dsDNA. The DNA-binding location (at the open DNA end or internal regions of the DNA molecule) of the wild-type M/R complex and the MR(Δcc) mutant on linear DNA in three different buffer conditions was determined using Scanning Probe Image Processor (SPIP) software (Image Metrology A/S): the distance between the protein complex and the open DNA end was measured by drawing a multipoint line along the corresponding DNA part and the software displays the covered distance in nanometers. If the protein complex binds at the end of the linear DNA molecule, the distance is 0 nm. Any distance above 0 nm counts as an internal location along the DNA substrate. When measuring the internal binding location along the linear DNA substrate (with two open DNA ends), the shorter of the two distances between bound protein and open DNA was taken into account. Individual Student *t* tests and a Kruskal–Wallis ANOVA on ranks in combination with the Dunn's test (66) were applied to check the statistical significance of the results.

Electrophoretic Mobility-Shift Assays. Linear 400 bp dsDNA substrate (at 6.25 nM) was mixed with 0, 7.5, 15, or 30 mg of the Zn231 Rad50 protein in a total reaction volume of 100 mL EMSA buffer (50 mM potassium acetate, 20 mM Tris-acetate at pH 8, 10 mM magnesium acetate, 100 mM NaCl, 5% glycerol, 1 mM dithiothreitol (DTT) for 15 min at 60 °C . Products were resolved on 5% polyacrylamide gels in 1× Tris-borate-EDTA and visualized with SYBR Gold stain (Thermo Fisher); full methodology is provided in *SI Appendix*.

ATP-Dependent DNA Unwinding by M/R. A total of 6.5 nM of wild-type or mutant M/R, and 0.2 nM linear DNA were incubated at 60 °C for 15 min in reaction buffer (50 mM potassium acetate, 20 mM Tris-acetate, 10 mM magnesium acetate, 150 mM NaCl, 0.05 mM zinc chloride, pH 8) in the presence or absence of 3 mM ATP or 3 mM nonhydrolyzable AMP-PNP, and imaged in air on nickel-modified mica. A control sample without M/R plus 3 mM ATP was also prepared at 60 °C. Activity was also tested in the presence of ATP at 45 °C and lower temperatures (37 °C and 25 °C) for 15 min and visualized by AFM imaging in dry conditions (*SI Appendix*, Table S4). A total of 100 DNA molecules were examined per condition; full details are provided in *SI Appendix*.

S1 Nuclease Digestion of M/R Unwound dsDNA. A total of 1.2 mM M/R complex was incubated with a 3-kb dsDNA substrate at 10.4 nM at 60 °C for either 4 or 10 min in reaction buffer (37.5 mM potassium acetate, 15 mM Tris-acetate at pH 8, 5 mM Tris-Cl at pH 8, 10 mM magnesium acetate, 75 mM NaCl, 1.25% glycerol, 1 mM DTT). Then 4 mL 5× S1 nuclease buffer plus or minus 2 mL S1 nuclease (Thermo Fisher, 100 U/mL) was added for 3 min at 60 °C. Following addition of sodium dodecyl sulfate at 1% and proteinase K at 1 mg/mL at 37 °C for 30 min, the DNA products were separated on a 0.8% agarose gel and visualized with ethidium bromide; full methodology is provided in *SI Appendix*.

Sample Preparation for AFM Imaging in Air. For AFM imaging in air, 15 mM nickel chloride (NiCl$_2$) was added to each sample, the solution was carefully mixed, then immediately deposited onto freshly cleaved mica and incubated for 5 min. The sample was washed eight times with 1 mL BioPerformance Certified (BPC) water and dried under a stream of nitrogen gas.

AFM Imaging and Data Analysis. All dry and fluid samples were imaged using the Dimension FastScan Bio Atomic Force Microscope (Bruker) in tapping mode.

For dry imaging, FastScan A probes (Bruker) with a spring constant of 18 N/m were tuned to a resonance frequency between 800 and 2,000 kHz and the amplitude setpoint was adjusted to the highest possible setting, so as to ensure little noise and minimizes the force the sample is exposed to. In fluid, FastScan D probes were used, with a spring constant of 0.25 N/m (resonance frequency of 90 to 140 kHz).

Fast-scan images were captured with a scan area of 1 to 2 μm, a scan rate of 15.1 Hz, and with 512 samples per line. For conventional AFM, images were captured at 1.8 frames per minute at room temperature.

Rad50 coiled-coil interactions with the DNA substrate during fast-scan imaging in fluid, as presented in Fig. 4A, were identified manually using similar interactions observed from AFM imaging in air data (Fig. 3) as a reference; see *SI Appendix* for further details.

All AFM images presented, excluding Fig. 6C, were processed using the Nanoscope Analysis software version 1.5 by Bruker Corporation. Fig. 6C was processed using SPIP software. Movies were produced using Windows Movie Maker.

Tracking the DNA Movement on the Mica Surface. The ImageJ software together with the JFilament Plugin (67) was used to track the position of DNA on the mica surface in a series of images captured during AFM imaging in fluid conditions. A multipoint line is drawn along the contour of the DNA filament. The x,y coordinates of each line were saved and displayed.

Molecular Simulation. A standard classical MD protocol of 100 ns was carried out, with five repeats. The protocols, structures, and entire input scripts appear in *SI Appendix*.

Data Availability. Raw data associated with this paper have been deposited in the Apollo, University of Cambridge Repository (https://doi.org/10.17863/CAM.50188).

1. J. K. Blackwood et al., End-resection at DNA double-strand breaks in the three domains of life. *Biochem. Soc. Trans.* **41**, 314–320 (2013).
2. D. S. Shin, A. J. Pratt, J. A. Tainer, Archaeal genome guardians give insights into eukaryotic DNA replication and damage response proteins. *Archaea* **2014**, 206735 (2014).
3. G. J. Williams, S. P. Lees-Miller, J. A. Tainer, Mre11-Rad50-Nbs1 conformations and the control of sensing, signaling, and effector responses at DNA double-strand breaks. *DNA Repair* **9**, 1299–1306 (2010).
4. C. B. Schiller, F. U. Seifert, C. Linke-Winnebeck, K.-P. Hopfner, Structural studies of DNA end detection and resection in homologous recombination. *Cold Spring Harb. Perspect. Biol.* **6**, a017962 (2014).
5. J. C. Connelly, D. R. F. Leach, Tethering on the brink: The evolutionarily conserved Mre11-Rad50 complex. *Trends Biochem. Sci.* **27**, 410–418 (2002).
6. R. S. Williams, J. S. Williams, J. A. Tainer, Mre11-Rad50-Nbs1 is a keystone complex connecting DNA repair machinery, double-strand break signaling, and the chromatin template. *Biochem. Cell Biol.* **85**, 509–520 (2007).
7. A. Syed, J. A. Tainer, The MRE11-RAD50-NBS1 complex conducts the orchestration of damage signaling and outcomes to stress in DNA replication and repair. *Annu. Rev. Biochem.* **87**, 263–294 (2018).
8. M. Lisby, J. H. Barlow, R. C. Burgess, R. Rothstein, Choreography of the DNA damage response: Spatiotemporal relationships among checkpoint and repair proteins. *Cell* **118**, 699–713 (2004).
9. R. S. Maser, K. J. Monsen, B. E. Nelms, J. H. J. Petrini, hMre11 and hRad50 nuclear foci are induced during the normal cellular response to DNA double-strand breaks. *Mol. Cell. Biol.* **17**, 6087–6096 (1997).
10. M. van den Bosch, R. T. Bree, N. F. Lowndes, The MRN complex: Coordinating and mediating the response to broken chromosomes. *EMBO Rep.* **4**, 844–849 (2003).
11. J. Lafrance-Vanasse, G. J. Williams, J. A. Tainer, Envisioning the dynamics and flexibility of Mre11-Rad50-Nbs1 complex to decipher its roles in DNA replication and repair. *Prog. Biophys. Mol. Biol.* **117**, 182–193 (2015).
12. K.-P. Hopfner et al., Structural biochemistry and interaction architecture of the DNA double-strand break repair Mre11 nuclease and Rad50-ATPase. *Cell* **105**, 473–485 (2001).
13. R. S. Williams et al., Mre11 dimers coordinate DNA end bridging and nuclease processing in double-strand-break repair. *Cell* **135**, 97–109 (2008).
14. D. Das et al., Crystal structure of the first eubacterial Mre11 nuclease reveals novel features that may discriminate substrates during DNA repair. *J. Mol. Biol.* **397**, 647–663 (2010).
15. K. Lammens et al., The Mre11:Rad50 structure shows an ATP-dependent molecular clamp in DNA double-strand break repair. *Cell* **145**, 54–66 (2011).
16. H. S. Lim, J. S. Kim, Y. B. Park, G. H. Gwon, Y. Cho, Crystal structure of the Mre11-Rad50-ATPγS complex: Understanding the interplay between Mre11 and Rad50. *Genes Dev.* **25**, 1091–1104 (2011).
17. R. A. Deshpande et al., ATP-driven Rad50 conformations regulate DNA tethering, end resection, and ATM checkpoint signaling. *EMBO J.* **33**, 482–500 (2014).
18. E. Kinoshita, E. van der Linden, H. Sanchez, C. Wyman, RAD50, an SMC family member with multiple roles in DNA break repair: How does ATP affect function? *Chromosome Res.* **17**, 277–288 (2009).
19. K.-P. Hopfner, J. A. Tainer, Rad50/SMC proteins and ABC transporters: Unifying concepts from high-resolution structures. *Curr. Opin. Struct. Biol.* **13**, 249–255 (2003).
20. P. Kalitsis, T. Zhang, K. M. Marshall, C. F. Nielsen, D. F. Hudson, Condensin, master organizer of the genome. *Chromosome Res.* **25**, 61–76 (2017).
21. T. Gligoris, J. Löwe, Structural insights into ring formation of cohesin and related Smc complexes. *Trends Cell Biol.* **26**, 680–693 (2016).
22. P. L. Graumann, T. Knust, Dynamics of the bacterial SMC complex and SMC-like proteins involved in DNA repair. *Chromosome Res.* **17**, 265–275 (2009).
23. F. Uhlmann, SMC complexes: From DNA to chromosomes. *Nat. Rev. Mol. Cell Biol.* **17**, 399–412 (2016).
24. K.-P. Hopfner et al., The Rad50 zinc-hook is a structure joining Mre11 complexes in DNA recombination and repair. *Nature* **418**, 562–566 (2002).
25. J. J. Griese, G. Witte, K.-P. Hopfner, Structure and DNA binding activity of the mouse condensin hinge domain highlight common and diverse features of SMC proteins. *Nucleic Acids Res.* **38**, 3454–3465 (2010).
26. A. Chiu, E. Revenkova, R. Jessberger, DNA interaction and dimerization of eukaryotic SMC hinge domains. *J. Biol. Chem.* **279**, 26233–26242 (2004).
27. M. Hirano, T. Hirano, Opening closed arms: Long-distance activation of SMC ATPase by hinge-DNA interactions. *Mol. Cell* **21**, 175–186 (2006).

28. M. de Jager et al., Differential arrangements of conserved building blocks among homologs of the Rad50/Mre11 DNA repair protein complex. *J. Mol. Biol.* **339**, 937–949 (2004).

29. R. S. Williams, J. A. Tainer, A nanomachine for making ends meet: MRN is a flexing scaffold for the repair of DNA double-strand breaks. *Mol. Cell* **19**, 724–726 (2005).

30. F. Moreno-Herrero et al., Mesoscale conformational changes in the DNA-repair complex Rad50/Mre11/Nbs1 upon binding DNA. *Nature* **437**, 440–443 (2005).

31. Y.-M. Soh et al., Molecular basis for SMC rod formation and its dissolution upon DNA binding. *Mol. Cell* **57**, 290–303 (2015).

32. L. R. Myler et al., Single-molecule imaging reveals how Mre11-Rad50-Nbs1 initiates DNA break repair. *Mol. Cell* **67**, 891–898.e4 (2017).

33. M. de Jager, C. Wyman, D. C. van Gent, R. Kanaar, DNA end-binding specificity of human Rad50/Mre11 is influenced by ATP. *Nucleic Acids Res.* **30**, 4425–4431 (2002).

34. M. de Jager et al., Human Rad50/Mre11 is a flexible complex that can tether DNA ends. *Mol. Cell* **8**, 1129–1135 (2001).

35. L. S. Shlyakhtenko, A. A. Gall, Y. L. Lyubchenko, Mica functionalization for imaging of DNA and protein-DNA complexes with atomic force microscopy. *Methods Mol. Biol.* **931**, 295–312 (2013).

36. K. P. Hopfner, C. D. Putnam, J. A. Tainer, DNA double-strand break repair from head to tail. *Curr. Opin. Struct. Biol.* **12**, 115–122 (2002).

37. B. Cannon et al., Visualization of local DNA unwinding by Mre11/Rad50/Nbs1 using single-molecule FRET. *Proc. Natl. Acad. Sci. U.S.A.* **110**, 18868–18873 (2013).

38. T. T. Paull, M. Gellert, Nbs1 potentiates ATP-driven DNA unwinding and endonuclease cleavage by the Mre11/Rad50 complex. *Genes Dev.* **13**, 1276–1288 (1999).

39. Y. Liu et al., ATP-dependent DNA binding, unwinding, and resection by the Mre11/Rad50 complex. *EMBO J.* **35**, 743–758 (2016).

40. W. Xu et al., A real time S1 assay at neutral pH based on graphene oxide quenched fluorescence probe. *Sens. Biosensing Res.* **7**, 42–47 (2016).

41. T. E. Melby, C. N. Ciampaglio, G. Briscoe, H. P. Erickson, The symmetrical structure of structural maintenance of chromosomes (SMC) and MukB proteins: Long, antiparallel coiled coils, folded at a flexible hinge. *J. Cell Biol.* **142**, 1595–1604 (1998).

42. K.-P. Hopfner et al., Mre11 and Rad50 from Pyrococcus furiosus: Cloning and biochemical characterization reveal an evolutionarily conserved multiprotein machine. *J. Bacteriol.* **182**, 6036–6041 (2000).

43. K. P. Hopfner et al., Structural biology of Rad50 ATPase: ATP-driven conformational control in DNA double-strand break repair and the ABC-ATPase superfamily. *Cell* **101**, 789–800 (2000).

44. D. E. Anderson, K. M. Trujillo, P. Sung, H. P. Erickson, Structure of the Rad50 x Mre11 DNA repair complex from Saccharomyces cerevisiae by electron microscopy. *J. Biol. Chem.* **276**, 37027–37033 (2001).

45. A. Rose, S. J. Schraegle, E. A. Stahlberg, I. Meier, Coiled-coil protein composition of 22 proteomes–differences and common themes in subcellular infrastructure and traffic control. *BMC Evol. Biol.* **5**, 66 (2005).

46. E. Kinoshita, S. van Rossum-Fikkert, H. Sanchez, A. Kertokalio, C. Wyman, Human RAD50 makes a functional DNA-binding complex. *Biochimie* **113**, 47–53 (2015).

47. C. Möckel, K. Lammens, A. Schele, K.-P. Hopfner, ATP driven structural changes of the bacterial Mre11:Rad50 catalytic head complex. *Nucleic Acids Res.* **40**, 914–927 (2012).

48. S. Sung et al., DNA end recognition by the Mre11 nuclease dimer: Insights into resection and repair of damaged DNA. *EMBO J.* **33**, 2422–2435 (2014).

49. M. de Jager et al., DNA-binding and strand-annealing activities of human Mre11: Implications for its roles in DNA double-strand break repair pathways. *Nucleic Acids Res.* **29**, 1317–1325 (2001).

50. T. T. Paull, M. Gellert, A mechanistic basis for Mre11-directed DNA joining at micro-homologies. *Proc. Natl. Acad. Sci. U.S.A.* **97**, 6409–6414 (2000).

51. J.-H. Lee et al., Ataxia telangiectasia-mutated (ATM) kinase activity is regulated by ATP-driven conformational changes in the Mre11/Rad50/Nbs1 (MRN) complex. *J. Biol. Chem.* **288**, 12840–12851 (2013).

52. J. Adamcik, J. H. Jeon, K. J. Karczewski, R. Metzler, G. Dietler, Quantifying supercoiling-induced denaturation bubbles in DNA. *Soft Matter* **8**, 8651–8658 (2012).

53. J. C. Bell, S. C. Kowalczykowski, RecA: Regulation and mechanism of a molecular search engine. *Trends Biochem. Sci.* **41**, 491–507 (2016).

54. E. M. Seitz, J. P. Brockman, S. J. Sandler, A. J. Clark, S. C. Kowalczykowski, RadA protein is an archaeal RecA protein homolog that catalyzes DNA strand exchange. *Genes Dev.* **12**, 1248–1253 (1998).

55. P. Sung, L. Krejci, S. Van Komen, M. G. Sehorn, Rad51 recombinase and recombination mediators. *J. Biol. Chem.* **278**, 42729–42732 (2003).

56. S. Van Komen, G. Petukhova, S. Sigurdsson, S. Stratton, P. Sung, Superhelicity-driven homologous DNA pairing by yeast recombination factors Rad51 and Rad54. *Mol. Cell* **6**, 563–572 (2000).

57. D. Ristic, C. Wyman, C. Paulusma, R. Kanaar, The architecture of the human Rad54-DNA complex provides evidence for protein translocation along DNA. *Proc. Natl. Acad. Sci. U.S.A.* **98**, 8454–8460 (2001).

58. W.-D. Heyer, X. Li, M. Rolfsmeier, X.-P. Zhang, Rad54: The Swiss Army knife of homologous recombination? *Nucleic Acids Res.* **34**, 4115–4125 (2006).

59. A. V. Mazin, C. J. Bornarth, J. A. Solinger, W. D. Heyer, S. C. Kowalczykowski, Rad54 protein is targeted to pairing loci by the Rad51 nucleoprotein filament. *Mol. Cell* **6**, 583–592 (2000).

60. L. A. Uranga, E. D. Reyes, P. L. Patidar, L. N. Redman, S. L. Lusetti, The cohesin-like RecN protein stimulates RecA-mediated recombinational repair of DNA double-strand breaks. *Nat. Commun.* **8**, 15282 (2017).

61. N. J. Rzechorzek et al., Structure of the hexameric HerA ATPase reveals a mechanism of translocation-coupled DNA-end processing in archaea. *Nat. Commun.* **5**, 5506 (2014).

62. J. K. Blackwood et al., Structural and functional insights into DNA-end processing by the archaeal HerA helicase-NurA nuclease complex. *Nucleic Acids Res.* **40**, 3183–3196 (2012).

63. L. S. Symington, Mechanism and regulation of DNA end resection in eukaryotes. *Crit. Rev. Biochem. Mol. Biol.* **51**, 195–212 (2016).

64. Y. L. Lyubchenko, L. S. Shlyakhtenko, A. A. Gall, *DNA-Protein Interactions* **543**, 337–351 (2009).

65. S. W. Schneider, J. Lärmer, R. M. Henderson, H. Oberleithner, Molecular weights of individual proteins correlate with molecular volumes measured by atomic force microscopy. *Pflugers Arch.* **435**, 362–367 (1998).

66. O. J. Dunn, Multiple comparisons among means. *J. Am. Stat. Assoc.* **56**, 52–64 (1961).

67. M. B. Smith et al., Segmentation and tracking of cytoskeletal filaments using open active contours. *Cytoskeleton* **67**, 693–705 (2010).

BIOCHEMISTRY